Modelling and monitoring the response of bonded composite/metallic structures during manufacturing process and damage evolution

A. Airoldi*, P. Bettini, S. Fournier, G.M. Capizzi, M. Stella
Dept. of Aerospace Science and Technlogy, Politecnico di Milano - Via La Masa, 34 – 20156 - Milano
ITALY
P. Bogotto
Aerea S.p.A. – Via C. Cattaneo, 24 – 22078 - Turate (CO)
ITALY

*alessandro.airoldi@polimi.it

ABSTRACT

The paper proposes experimental and numerical approaches to investigate and characterize delamination phenomena at the interfaces between carbon fibre reinforced composite laminates and layers of titanium alloy, obtained through co-cured and co-bonding process. The build-up of thermal residual stress between the different materials is controlled by properly designing specimens suited to be adopted in fracture mechanics experiments, such as Double Cantilever Beam (DCB) or End Notched Fracture tests (ENF). Manufacturing process is monitored through the insertion of strain sensors carried by optical fibres, which are subsequently used to monitor the strain evolution during DCB tests, performed with two different types of specimens. Numerical models are developed for the estimation of thermal stress during the cooling phase of manufacturing process and of the mechanical response in fracture tests. The results confirm that the proposed specimens can control the development of distortions due to the mismatch of coefficients of thermal expansion and point out capabilities and limits of simplified linear numerical approaches to capture the development of strains and stress during the cooling phase of manufacturing process. The optical fibre based monitoring system successfully monitored both the manufacturing process and the evolution of internal strains during the development of interface damage. A complete numerical approach is developed, by using multistep explicit analyses to carry out simulation of fracture propagation after an evaluation of thermal stress in the structure. The approach is validated in terms of overall force vs. displacement responses and local strain evolutions at the locations monitored by internal strain sensors.

1.0 INTRODUCTION

Hybrid structures made of different materials often represent optimal solutions to meet severe engineering requirements concerning stiffness, strength, fatigue, protection from impacts or thermal loads. In particular, the development of composite/metallic structural parts is studied to overcome some typical limitations of laminates made of long fibre reinforced plastics, such as carbon fibre reinforced composites, which have become a reference material for thin walled modern aerospace constructions due to their excellent structural efficiency in the plane of reinforcements fibres. However, such structural elements are not particularly adequate to carry three-dimensional stress states, are typically more brittle than metallic alloys and prone to intralaminar and interlaminar damage accumulation, and are more sensitive to environmental conditions and to the stress concentrations due to notches, cut-outs and geometric variations which are often required for connections, constraining and load application. For these reasons, metallic/composite hybrid structures have been considered for many applications, such as in Fibre Metal Laminates (FML) which exhibit superior fatigue and damage tolerance performances [1], in hybrid composite/metallic shafts with high torque transmission capability [2, 3], and in lightweight carbon control rods with Titanium terminals [4]. Moreover, metal inserts have been studied to enhance the strength of bolted joints in carbon composite panels [5-8] and

to apply concentrated loads in composite parts produced by Resin Transfer Moulding [9]. Nowadays, the increasing interest and the recent developments in additive manufacturing techniques suggest that hybrid structures will represent a diffused solution for future generations of highly efficient vehicle structures. In the military field, where operational conditions often include severe requirements regarding survivability in harsh environmental conditions and battle scenarios, the combination of fibre-reinforced composite parts and metallic elements could lead to enhance structural performances with innovative solutions, also based on the more complex geometries that could be produced by using additive manufacturing techniques.

Joining between metallic and composite constituent parts of a composite/metallic hybrid structural element can be achieved with several methods, which can be classified into mechanical joints, adhesively-bonded joints, and co-cured joints. Co-curing is the simplest method, since adhesion is obtained by exploiting an excess of resin in the pre-preg during the curing process of the composite part of the hybrid structure, without requiring additional materials. Adhesively bonded joints can also be obtained during the curing of the composite, but requires the interposition of an adhesive layer between the composite and the metallic parts. Such a type of process is denoted as co-bonding, whereas the joining of a pre-cured composite part to a metallic element in a subsequent, separate process is often referred to as secondary bonding. In general, all such methods could be more structurally efficient with respect to mechanical joints, which require drilling, involve the presence of cut-outs and stress concentrations, and the additional weight of rivets or bolts. However, two major issues characterize the application of adhesively bonded joints and co-cured joints, namely the development of thermal stress due to the mismatch of Coefficient of Thermal Expansions (CTE's) and the difficulties involved in the detection of damage at the interface between the adherends, which tends to grow under the action of operational loads and eventually leads to a catastrophic failure.

The development of thermal residual stress and of distortions during the curing process of composite parts have been extensively considered in literature [10-12] and are generally attributed to the mismatch between the CTE's of different materials or of orthotropic layers, to the chemical shrinkage during curing and to the frictional effects between the parts and the moulds. In hybrid composite/metallic structures, thermal stress build-up is a fundamental issue which can be mitigated by applying compressive pre-stress to composite parts [2,3] or by developing special curing cycles [13,14]. Despite the complexity of the phenomenon, acceptable numerical-experimental correlations have been obtained by analytical and numerical models where linear elastic material models and constant CTE have been used, provided that a zero-stress free temperature is identified [2, 15-17]. More accuracy can be obtained by introducing a temperature dependence of composite CTE's in matrix-dominated direction [18].

Different methods can be used to quantify thermal residual stresses in hybrid or composite structures [12,19], including the possibility of embedding, in the composite materials, optical fibres carrying Fibre Bragg Gratings sensors (FBG), which can provide both measures of strain and temperature [18,20]. The adoption of optical fibre-based sensing networks is particularly appealing since it can also represent a possible solution to detect the development of interface damage in critical regions, during the operational life of the structure, as it has been proved by a large number of applications [20,21]. Optical fibres can be embedded in a composite at a certain distance from the interface where damage has developed and can detect anomalies in the internal strain field under the action of applied loads [22, 23]. Moreover, damage can cause the release of thermal stress accumulated during manufacturing process, so that anomalies in the strain fields are also detectable in unloaded conditions. The prediction of such phenomenon is of fundamental importance to design health monitoring networks which can detect sub-critical damage at the critical interfaces of hybrid structures. Such aspect is particularly important when load conditions cannot be accurately predicted in advance and when the need for an efficient and fast monitoring of structural integrity is a fundamental issue, as in the case of military vehicles.

Following the aforementioned considerations, the paper is aimed at providing methods to characterize, monitor and model junctions between metallic and composite parts, considering two types of interfaces between carbon reinforced composites and titanium alloy plates, namely a co-cured junction between a

laminate made of fabric plies and a co-bonded junction with unidirectional laminates. All the presented activities are focused on specimens and tests for the characterization of interface toughness, which is indeed a fundamental property to guarantee the structural integrity and the damage tolerance of the hybrid structure. However, since the fracture toughness tests measure the energy required to separate the interfaces, the level of thermal stress and thermally induced distortions in the specimens must be carefully controlled, to avoid that the release of the stress and the recovery of distortions, and the consequent energy release, may affect the results. Therefore, a first issue is represented by the design of specimens that can be subjected to debonding tests without undesired release of the energy stored with the build-up of thermal residual stress. Manufacturing of such specimens has been carried out also considering the embedment of optical fibres, with FBG sensors at prescribed locations, installed to monitor both strain and temperature during manufacturing process and evolution of strain during fracture tests. The design of specimens and of the sensing network are presented in the subsequent section of the paper. In the following section, monitoring of manufacturing processes and experimental activities on Double Cantilever Beam (DCB) tests to measure fracture toughness in mode I opening are discussed. Thereafter finite element models are developed to predict the level of thermal stress, by using a linear approach, and the forces required to open the junction in mode I, with a non-linear approach based on cohesive elements, which is validated also considering the strain evolution inside the composite. Finally, a complete multi-step approach is presented to model, within the same analysis, both the thermal stress and the potential distortion development during cooling, and the damage development at interfaces under the action of external loads. Such numerical approach completes the assessment of a set of experimental and numerical tools that can be used to characterize, investigate, monitor and predict the response of interfaces in hybrid structures.

2.0 SPECIMEN AND SENSING NETWORK DESING AND MANUFACTURING

2.1 Design of specimens for the characterization of hybrid interface toughness

Double Cantilever Beam (DCB) and End Notched Flexure (ENF) tests, are typically used to evaluate the fracture toughness of interfaces in composite materials and have been originally conceived to be used with homogeneous lamination sequences. The DCB test specimen, sketched in Fig. 2-1-A, consists of a laminate pre-cracked at the mid-plane, in correspondence of the interface whose toughness has to be evaluated. Application of such type of test for the characterization of interfaces in hybrid structures is not straightforward, since specimens are inherently inhomogeneous and data reduction methods used to evaluate toughness from test response can lose their validity. Indeed, non-linear numerical approaches based on cohesive zone models [22,23] can be nowadays used to efficiently model DCB and ENF tests, so that toughness property evaluation could be performed by numerical identification procedures even for non-conventional lay-ups. However, the development of thermal stresses and distortions in the hybrid laminate represents an additional difficulty, which furtherly complicate the evaluation of the energy required to propagate interface damage.

In this work, interfaces between layers of a Ti-6AL-4V Titanium alloy and two types of carbon reinforced composite layers, with unidirectional IM7 fibres and 5H-style AS4 fabric reinforcement have been tested. Both composite pre-pregs are characterized by the same Hexcel 8552 epoxy matrix,
The specimens adopted have been designed with the aim of eliminating, or minimizing at a negligible level, the effects of the thermal stress release during fracture testing, so that a reliable estimation of toughness can be carried out. To accomplish such objective, the lamination sequences of the whole specimen and of the two arms separated by the pre-cracked interface have been determined following three fundamental criteria:

- symmetric lay-up for the two arms of the DCB specimens, to avoid bending-extension coupling and consequent curvatures induced by cooling for the two semi-laminates separated by the joining interface;
- same volumetric fraction of composite materials and titanium alloy in both arms, so to achieve the same overall CTE in the two parts joined at the interface and avoid bending of the whole specimen;

- thickness of metallic and composite layers selected in order to achieve the same bending modulus of the two arms, so to achieve a symmetric response during DCB tests.

For specimen design, isotropic titanium alloy layers with a Young Modulus of 114 GPa, a Poisson's ratio of 0.34 and a CTE of $9 \cdot 10^{-6}$ C^{-1} have been considered, whereas the nominal properties of composite pre-pregs, as declared by the producer, are listed in Table 2-1.

		UD IM7-8552	FB AS4-5H-8852
ply thickness	Mm	0.131	0.195
E_1 (tension)	Gpa	164	68
E_1 (compression)	Gpa	150	60
E_2	Gpa	12	66
G_{12}	Gpa	5	5
ν_{12}	-	0.3	0.05
CTE_1	10^{-6} °C^{-1}	-0.3	2.1
CTE_2	10^{-6} °C^{-1}	28	2.1

Table 2-1: Nominal properties of composite plies for specimen design

The lay-up of the hybrid specimen selected to fulfil the aforementioned criteria is shown in Fig. 2-1-B, which consists of macro-layers with a thickness of about 1 mm or 2 mm for both the composite and metallic parts. Different possible configurations have been considered with different lay-ups of the composite parts, defined in order to fulfil the criteria with the prescribed thickness values.

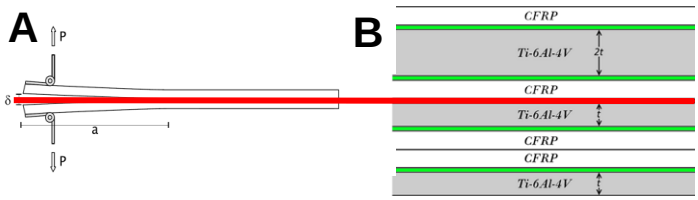

Figure 2-1: Lay-out of a DCB test (A) and lamination sequence of hybrid laminates (B)

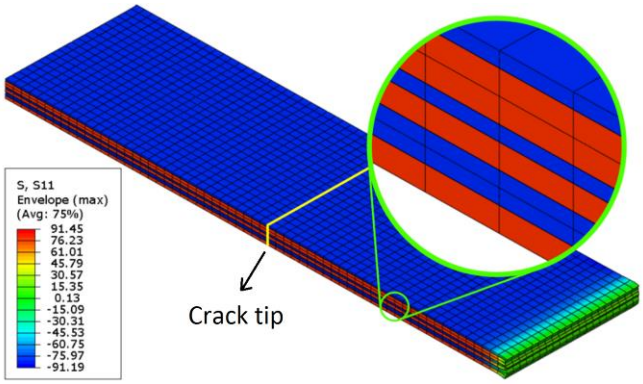

Figure 2-2: Contour of longitudinal normal stress in thermal finite element model for preliminary design of specimens

The expected responses of the hybrid laminates have been estimated by developing a thermal finite element model of laminates including a pre-crack between the arms, by using the properties presented in Table 2-1. A temperature variation from 180° C to 20° C has been uniformly imposed to all the specimens, with a linear

perturbation analysis. The Simulia/Abaqus Standard solver code has been used. The length and the width of the modelled laminates have been fixed to 300 mm and 80 mm, respectively, which are adequate to represent a laminate that has to be subsequently cut to produce fracture mechanics specimens. Thickness has been chosen according to the defined lay-ups. Second order solid elements C3D20R have been used, with 1.25 mm x 1.25 mm in-plane dimension. The model presented in Fig. 2-2 is referred to a part of the laminate and the stress contour presented is representative of the results obtained in the FE analyses, where a compressive stress state σ_{11}, in the longitudinal direction of the specimen, is achieved in the titanium alloy and a tensile stress state is obtained in the composite sub-laminates. It is worth noting that solutions are identical in the pre-cracked as well as in the joined parts, and that no distortion is predicted in the laminate, which undergoes a uniform shrinkage in the longitudinal, transverse and through the thickness directions during the simulation of the cooling process. Along the edges, interlaminar shear stress are developed at interfaces between composite sub-laminate and metallic layers. For the different solutions considered in the analyses, Table 2-2 provides the maximum stress values in the composite material and in the Titanium alloy. In the second solution, two 90° oriented plies have been included to better fulfil the sizing criteria, but it can be observed that very high thermal stress are achieved in such plies. Overall, the results of the preliminary sizing activity indicate that the homogenous sub-laminates made of unidirectional and fabric layers are feasible solutions to avoid distortions and properly characterize the toughness of interfaces. Moreover, the same type of specimens could be used to carry out significant experiments considering different load and environmental conditions, propagation modes and fracture development along interfaces not located at the mid-plane.

CFRP thick sub-laminate lay-up	layers	σ_{11} (MPa)
$^{UD}[0°]_7$	Ti-6Al-4V	+86.6
	$^{UD}[0°]$	-88.3
$^{UD}[0°]_5$ $^{UD}[90°]_2$	Ti-6Al-4V	+77.7
	$^{UD}[0°]$	-125
	$^{UD}[90°]$	-203
$^{FB}[0°]_5$	Ti-6Al-4V	+49.6
	$^{FB}[0°]$	-51.5
$^{FB}[0°]$ $^{UD}[0°]_6$	Ti-6Al-4V	+86
	$^{FB}[0°]$	-29
	$^{UD}[0°]$	-100

Table 2-2: Maximum thermal stress predicted by preliminary model

2.2 Manufacturing of sensorized laminates for DCB specimens

A strain and temperature sensing network based on FBG sensors carried by optical fibres has been embedded in the composite sub-laminate closer to the pre-cracked interface, to monitor strain and temperature evolution during manufacturing process and testing. Optical fibres have been introduced during the lamination of the specimen, in the interlaminar layer at a distance of two plies and one ply from the pre-crack interface for unidirectional and fabric sub-laminates, respectively, according to the same technique adopted in [20, 23]. Each fibre carries a different number of local FBG sensors, which reflect the light transmitted through the fibre at a variable wavelength, depending on temperature and strain experienced by the sensors, as shown in Fig. 2-3-A.

The objectives of the sensing network embedded in the produced hybrid laminate and specimens can be summarized in the following list:

- monitoring of temperature during the manufacturing process;
- monitoring of strain during the manufacturing process, and in particular of shrinkage due to CTE in

the cooling phase and of possible raising of distortions in hybrid elements; such data will also provide useful information to validate a numerical approach for the estimation of thermal stress build-up during manufacturing;

- monitoring of the evolution of strain in the vicinity of the crack during fracture testing, with the main aim of validating numerical model;
- monitoring of the residual strain in the specimens after crack propagation, which is expected to be negligible for the specific specimens considered in this work, when the pre-cracked interface is located at the mid-plane of the laminate.

The strain evolution during fracture testing has been monitored by sensors which are located along the optical fibres in the region in front of the pre-crack, as shown in Fig. 2-3-B. The specimens are cut from laminates that are cured in a heat plate press, by using a rectangular mould that makes possible the production of several specimens having a width of 25 mm and a length of 250 mm, sketched in Fig. 2-3-C. In particular, the lay-out reported in Fig. 2-3-C leads to the production of six specimens, four of the them sensorized by optical fibres. The four optical fibres carrying the FBG sensors that will be used both for process monitoring and strain monitoring in DCB specimens are drawn in red in Fig. 2-3-C. The potential of optical fibre-based sensing network for process and fracture monitoring is assessed by using two types of optical fibres embedded in the composite laminate. In the first type of fibres, the fibre core is protected by a polyacrylate coating, which is removed by chemical etching in correspondence of the position of 3 FBG sensors, positioned at a mutual distance of 50 mm. Coating removal, suggested by some authors [18] is aimed at providing an optimal transmission between the strain experienced by the resin of composite material and the fibre core. The adopted fibres have a diameter of 250 μm, including coating, and of 125 μm without coating. In the second type of fibre, with a diameter of 195 μm, coating is made of a ceramic material (Ormocer®) and it is not removed from the fibre at sensors locations. Such fibres are endowed with two FBG sensors at a distance of about 100 mm.

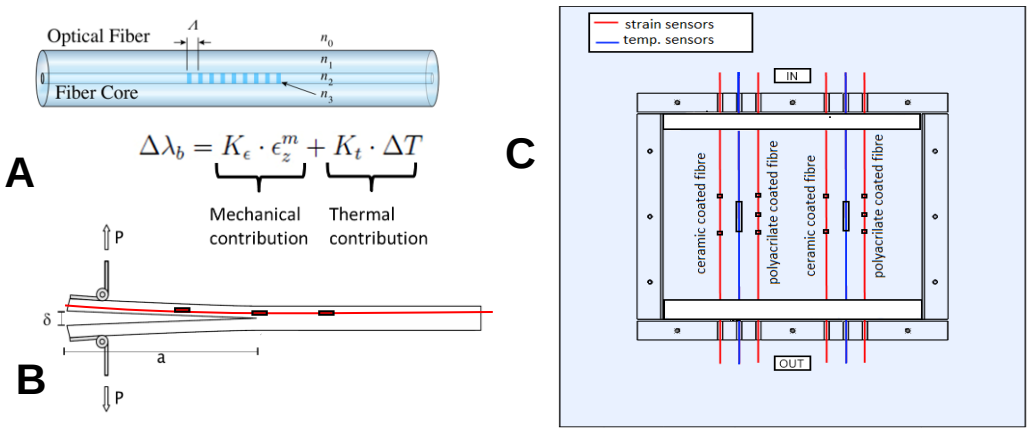

Figure 2-3: Fibre Bragg Grating inscribed on optical fibres (A), embedment of sensing system in a DCB specimen (B) and lay-out of sensing network in the laminate for DCB specimen production (C)

Additional optical fibres, drawn by using the blue lines in Fig. 2-3-C, are introduced in the laminate between two adjacent specimens, which are used to implement a direct measurement of temperature and to make possible a decoupling of mechanical and thermal contributions indicated in the equation included in Fig. 2-3-A. The adopted technique involves the passage of the optical fibre inside a steel capillary tube, where the fibre is loosely constrained and an FBG sensor is located, so that the strains experienced by the surrounding material cannot be transmitted to the FBG sensor, which becomes sensitive only to temperature [20, 24].

After some preliminary trials, two types of hybrid laminates have been produced and subsequently cut to obtain DCB specimens for interface fracture testing:

Type A) – Co-bonded hybrid specimens with unidirectional IM7-8552 sub-laminates having an homogeneous lay-up $[0]_n$, and anodized layers of Ti-6Al-4V alloy, bonded by means of a 3M™ Scotch-Weld AFK-163-2K adhesive.

Type B) – Co-cured hybrid specimens with $[0]_n$ AS4-5H-8552 fabric composite sub-laminates cured over anodized layers of Ti-6Al-4V alloy without the interposition of any adhesive layer.

The interfaces at the mid-planes of all the specimens are pre-cracked by introducing a PTFE sheet for a length of about 70 mm in the manufacturing process. It must be observed that the preliminary technological trials suggested to interpose adhesive layers at all the metal/composite interfaces of specimens type A, due to the risk of damage development at the weak (even if non pre-cracked) interfaces between unidirectional sub-laminates and titanium anodized layers. Hence, all the interfaces between composite layers and metallic sheets are actually co-bonded in type A specimen.

The pictures in Fig. 2.4 are referred to the manufacturing process of two Type B specimen. The metallic dams and the silicon rubber dams that constitutes the edges of the mould are visible in Fig. 2-4-A. Two optical fibres carrying the FBG sensors that will be embedded in DCB specimens are placed on the fabric layer adjacent to the pre-cracked interface, whereas, on the left side, the optical fibre introduced in the capillary tube is visible. Such fibre will be positioned between the fibres that have been already placed in the picture, after having cut the composite pre-preg in order to house the tube. After curing, a 5 mm wide zone where the capillary tube has been inserted is cut and discarded, so that the presence of the tube does not affect the properties of the DCB specimens. In Fig. 2-4-B a detail of fibre egress is shown: both the silicon and the metallic dams are cut to make possible the passage of the optical fibres, which can be interrogated during the process, carried out by positioning the hybrid lay-up in a heat plate press, and by applying a second aluminium plate on the upper surface of the laminate, with edges acting on the soft silicon rubber dam to seal the hybrid laminate during process.

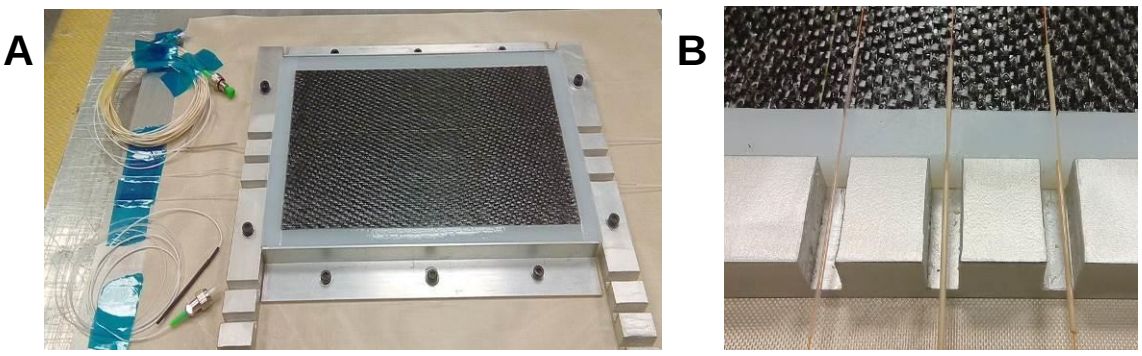

Figure 2-4: Manufacturing of hybrid panel with embedded optical fibres (A) and particular of optical fibre egress from the laminate and the mould (B)

3.0 MANUFACTURING MONITORING AND FRACTURE MECHANICS TESTING

3.1 Monitoring of manufacturing process

The FBG sensors hosted in the capillary tubes have been used to determine the temperature inside the hybrid laminate during the curing cycle. The temperatures measured in production cycles for the type A and type B

laminates are reported in Fig. 3-1-A and Fig. 3-1-B, respectively. Acquisitions cover a phase of introduction, adjustment and closure of the mould in the heat press plate apparatus, and two ramps of temperature, separated by a maintenance period of one hour. A final maintenance of 2 hours at 180°C and the cooling phase complete the cycles. FBG measures indicates that the internal temperature inside the hybrid laminates has accurately followed the prescribed cycles. The wavelength shift due to temperature has been subtracted from the total shift measured by the FBG sensors directly embedded in the resin of the composite sub-laminate to obtain the strain evolution during curing. The resulting evolution of strains is reported in Fig. 3-2, both for the three FBG sensors on the polyacrylate-coated optical line, with coating removed at FBG locations, and for the two FBG sensors on the ceramic-coated fibre, in the two types of laminates A and B.

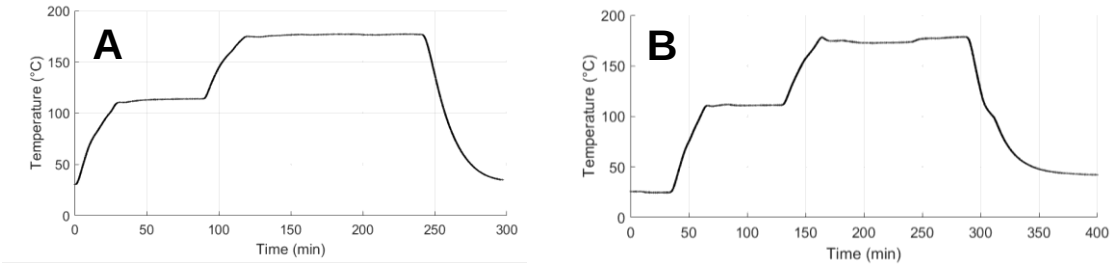

Figure 3-1: Temperature cycles for co-bonded hybrid unidirectional-Ti (A) and co-cured hybrid fabric-Ti (B) laminates

The strain evolution reported in Fig. 3-2-A is referred to laminate type A, with unidirectional sub-laminates. In the first minutes of the cycle, pressure is applied and this induced a different response on the polyacrylate-coated and ormocer-coated fibres. Thereafter, the sensors have followed similar trends. If initial offset is neglected, it can be seen that responses are indeed similar and that small strains have been developed until the cooling phase, which started after about 240 minutes from the beginning of the acquisition and is characterized by an apparent development of negative longitudinal strains. The strains obtained in the curing process of type B laminates, with fabric sub-laminates, are shown in Fig. 3-2-B. In this manufacturing process, the heat plate press has been closed and then immediately re-opened in the initial phase, thus originating the oscillations that are visible in the first 40 minutes of acquisitions. It has to be remarked that, in a such a phase, fibres are not actually bonded to the surrounding plies, so that the data provided can be difficulty interpreted. However, after the first temperature ramp, strains are quite similar at all FBG locations, but the application of the second temperature ramp led to a deviation between the strains acquired by the polyacrylate-coated fibre and the by the ormocer-coated fibre, which indicate a positive strain of about 200 με. Such offset is not recovered during the cooling phase, which clearly indicate the shrinkage of the specimen.

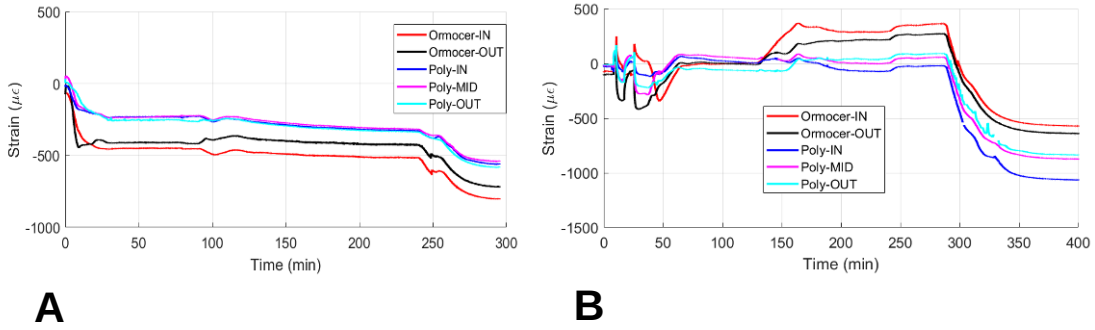

Figure 3-2: Strain evolution in the manufacturing process for co-bonded hybrid unidirectional-Ti (A) and co-cured hybrd fabric-Ti (B) laminates

Indeed, the strain measurement in the fabric sub-laminates is more complicated due to the presence of the mutually perpendicular yarns, which do not provide room for an optimal hosting of the optical fibre, whereas, in a unidirectional ply, reinforcement fibres can easily make room to host the optical element, by disposing around it, if they have the same direction. Accordingly, in the fabric laminate, the fibres are actually hosted in a pocket of resin that develops between two adjacent plies and yarns exert a non-negligible transversal pressure, which can alter the measure. Indeed, during the production of specimens with fabric sub-laminates, the splitting of the reflected light spectrum, which is an indication of optical fibre ovalization, has been detected for all the uncoated FBG sensors on the polyacrylate-coated fibre. Such phenomenon has not been observed in the other technological processes carried out in the activity.

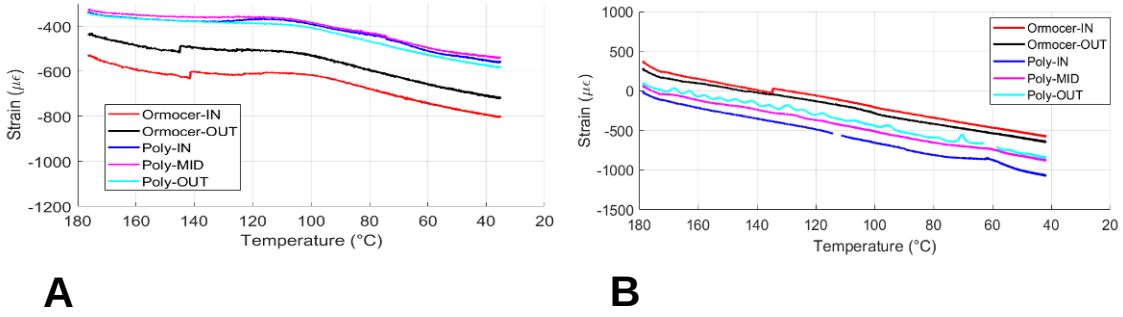

Figure 3-3: Strain vs. temperature curve in the cooling phase of the process for co-bonded hybrid unidirectional-Ti (A) and co-cured hybrd fabric-Ti (B) laminates

Despite the aforementioned issue, a significant result has been obtained by plotting the strain versus the temperature in the cooling phase of the process, as it is shown in Fig. 3-3. It can be observed that for both the types of laminate the trends and the slopes of strain vs. temperature curves are similar for all the sensors. In the results for the co-bonded hybrid laminate with unidirectional layers, shown in Fig- 3-3-A, the relation between strain and temperature is non-linear, although the sensors are set in the fibre direction, where CTE dependence from temperature should be relatively limited [18]. Such trend could indicate possible influence of the friction between the tool and the specimens, which opposes to the shrinkage, as well as of the viscous behaviour of the adhesive set between all the interfaces between metallic and composite parts. On the other hand, the result obtained by the co-cured fabric laminate exhibits a linear trend of the strain vs. temperature relation, as presented in Fig- 3-3-B, thus indicating a CTE substantially constant for the overall laminate. Moreover, the slope is quite similar for all the considered sensors. The results confirm that contraction in the longitudinal direction is higher in the presence of fabric sub-laminates and this is expected, since the lower volumetric fraction of fibre in such direction that opposes to the contraction of the metallic layer. The results obtained represent valuable data to validate a simplified thermal model of the cooling phase of the process, which can be used to estimate thermal stress development inside the laminate.

3.2 Experimental DCB testing

The laminates produced in manufacturing process described in the previous sub-section have been cut by means of a water-jet cutter to obtain three specimens for each laminate type, which have been tested according to the DCB procedure. The experiments have all been conducted by first performing a pre-opening phase, according to ASTM procedure [25], which has been used a guideline. Three specimens have been tested for each type of hybrid laminate, one sensorized with polyacrylate-coated fibres, another with ceramic-coated fibres and one without sensors. An MTS 858 hydraulic test system has been used for all the experiments. A test on a type A specimen and the detail of the crack tip is shown in Fig. 3-4, whereas a test on type B laminate is shown in Fig. 3-5. In the tests, damage apparently developed only the pre-cracked central interfaces, as it shown in Fig. 3-4-A and in the detail presented in Fig. 3-4-B for the unidirectional

specimens with adhesively bonded interface, where the reinforcing web embedded in the adhesive film can also be noticed. According to such results, the introduction of adhesive in all the metal/composite interfaces avoided the development of damage far from the central pre-cracked interface, which, on the contrary, was detected in preliminary tests performed on technological trials. In the type B specimens, with co-cured interfaces between the titanium alloy sheet and the fabric sub-laminate a neat fracture developed at the pre-cracked interface, as it is shown in Fig. 3-5, without signs of other types of damage at the other interfaces.

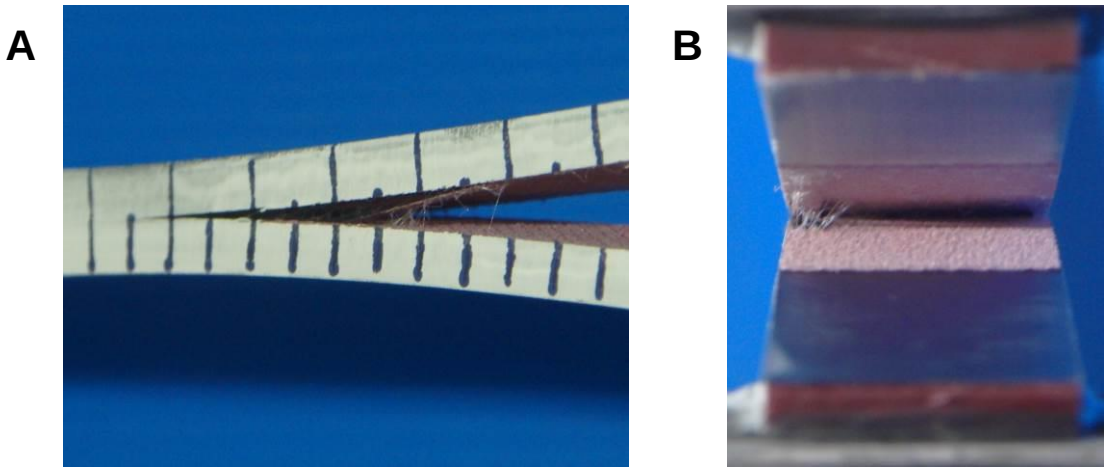

Figure 3-4: DCB experiment on a hybrid specimen with unidirectional sub-laminate (A), and detail of the crack tup (B)

The force vs. displacement responses are presented in Fig. 3-6-A and Fig. 3-6-B for the specimens type A and type B, respectively. The trends are qualitatively similar between the two type of hybrid specimens, and the scattering among the experiments performed on the same type of specimens is quite limited. No significant deviation from linearity can be observed in the initial phase of the test, thus confirming that the no unexpected inelastic phenomena occurred until the onset of crack propagation at the central interface. Moreover, a significant common feature of the response is the very limited level of residual displacements at the end of the unloading phase. Such aspect confirms the expected response of the quasi-symmetric hybrid laminates, which do not exhibit bending distortions before and after crack opening. However, a large quantitative difference is apparent between the response of co-bonded type A specimens and co-cured type B specimens, despite the thickness of the arms and their bending stiffness are similar, thus indicating that the toughness of co-cured interfaces between the fabric sub-laminate and the anodized titanium alloy sheets is significantly lower than the toughness achieved by using the adhesive layer.

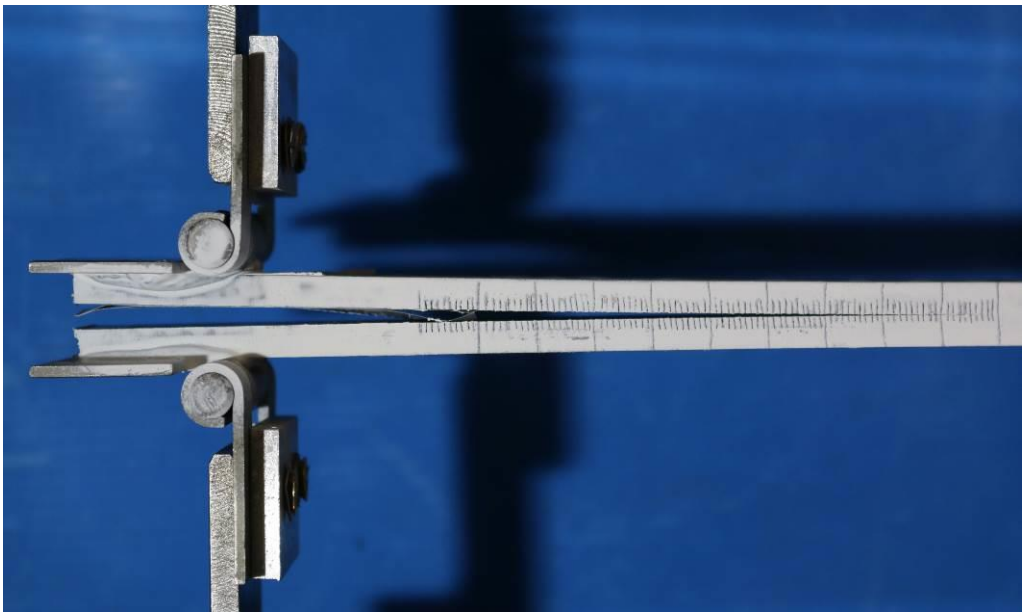

Figure 3-5: DCB experiment on a hybrid specimen with fabric sub-laminates

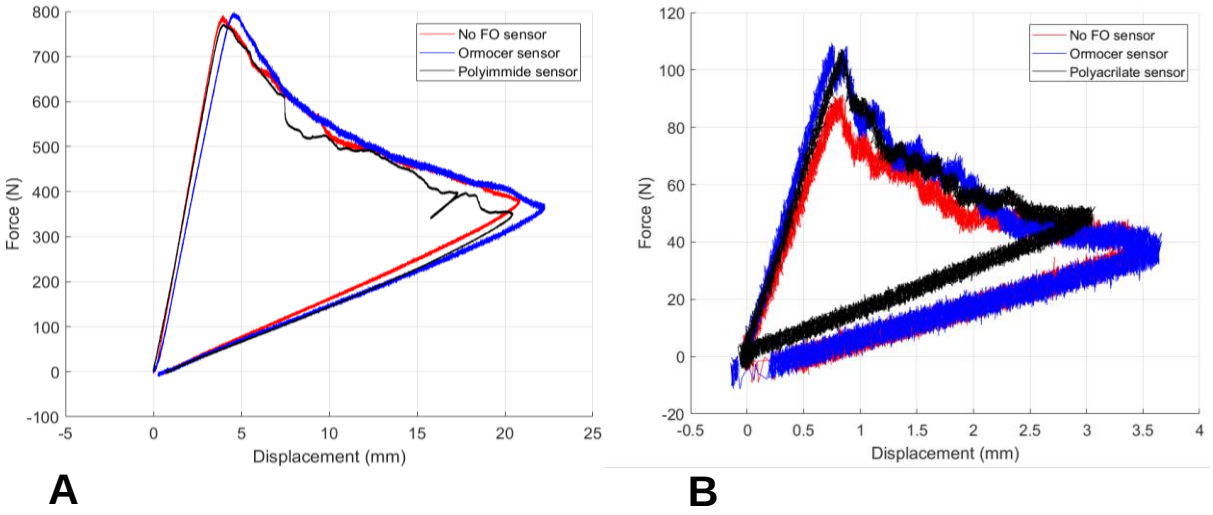

Figure 3-6: Force vs. displacement responses for hybrid specimens with unidirectional sub-laminates (A) and hybrid specimen with fabric sub-laminates (B)

The application of two data reduction methods suggested by ASTM standard [25], namely Modified Beam Theory (MBT) and Modified Compliance Calibration (MCC) to two type A specimens is shown in Fig. 3.7-A and Fig- 3-7-B. The Energy Release Rate (ERR) is evaluated for different crack lengths and it can be observed a slightly increasing trend for both specimen, with values raising from 2.8 kJ/m^2÷3.0 kJ/m^2 at the beginning of the test, until to values of 3.2 kJ/m^2÷3.4 kJ/m^2 after 60 mm of crack propagation, with an increment about 12%, which can be attributed to possible phenomena of fibre bridging during propagation. The application co-cured specimens with fabric sub-laminates of the two aforementioned reduction methods and of Compliance Calibration method (CC), as well suggested in [25], provide a toughness that is about two orders of magnitude lower, with values ranging for 0.04 kJ/m^2 to 0.08 kJ/m^2, as shown in Fig. 3-7-C and Fig. 3-7-D.

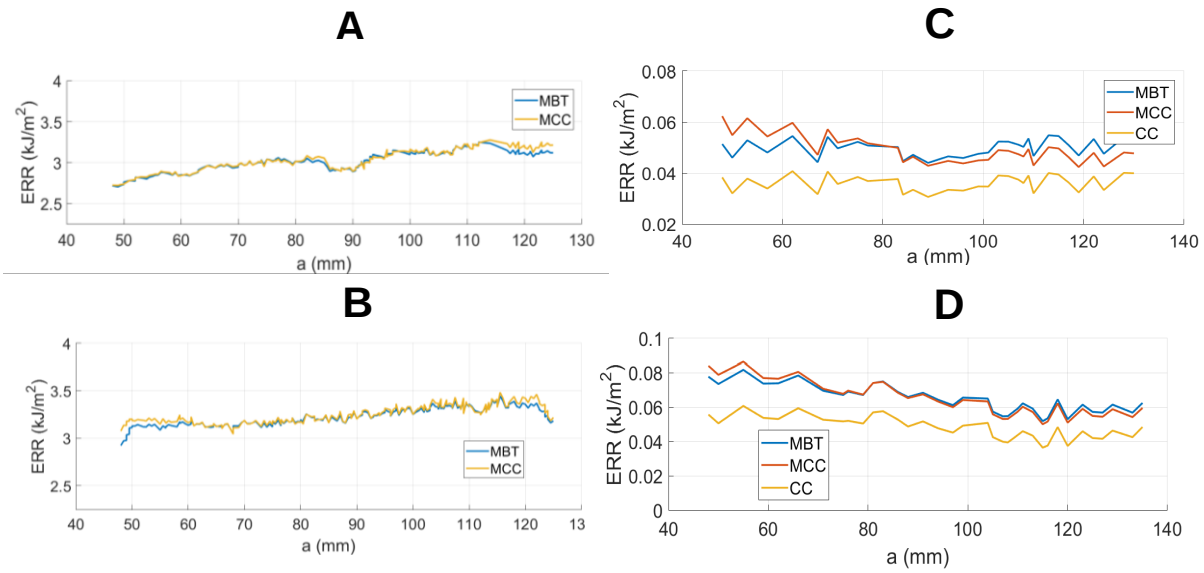

Figure 3-7: R-curves for co-bonded UD-Ti specimen without sensors (A), co-bonded UD-Ti with ormocer optical fibre (B), co-cured FB-Ti without sensors (C), and co-cured FB-Ti with ormocer optical fibre (D)

4.0 NUMERICAL MODELS

4.1 Simplified thermo-mechanical models for cooling process

The identification of thermal stress build-up during the manufacturing process is a challenging task that requires to take into account several aspects, such as the viscous response of polymeric materials, the effects of tools-specimens interactions, the variability of CTE with temperature. The approach followed in the present work is the development of a finite element model that can be used both for a rough estimation of the thermal stress and of the distortions consequent to curing cycle and also, in subsequent analyses, for the prediction of the local and global response in the presence of damage onset and propagation at the interfaces. The finite element model developed for the analyses is shown in Fig. 4-1. The mesh consists of brick elements (type C3D8R [26]) with approximate size of 0.5 mm x 0.5 mm x 0.5 mm, for a total number of about 300000 elements. In the model, which is prepared considering the application for fracture test analysis, a layer of cohesive elements (COH3D8 [26]) has been interposed between the elements representing the composite sub-laminates and the metal layers at the pre-cracked interface.

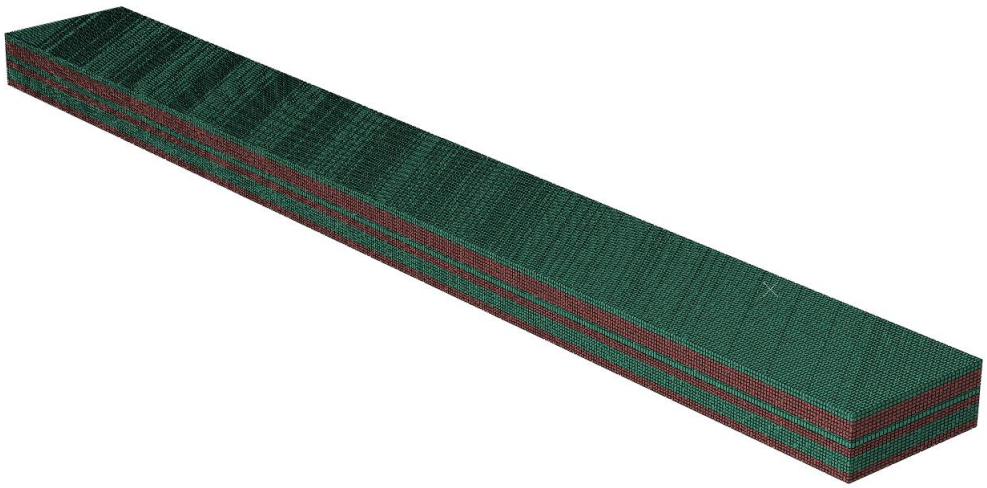

Figure 4-1: Finite element model developed for thermo-mechanical analyses

A simulation of cooling process has been conducted considering constant CTE's for the materials. The elastic properties used in the analyses are listed in table 4-1. They are obtained from the properties listed in Table 2-1 after a normalization that takes into account the ply thickness evaluated after the curing process, so that fibre-dominated properties have been re-scaled considering the variation in the fibre volumetric fraction. The largest variation that can be observed for unidirectional plies takes into account that, in the numerical model, the adhesive layer is not geometrically represented, although its thickness is not negligible (about 0.1 mm). Accordingly, the properties of composite plies have been diluted in the overall thickness of the sub-laminates, which also include the thickness of adhesive layers. The properties of titanium alloy have been kept equal to the ones adopted in preliminary analyses described in section 2.1.

		UD IM7-8552	FB AS4-5H-8852
E_1	GPa	133	71
E_2	GPa	12	71
E_2	GPa	12	10
G_{12}	GPa	5	5
G_{13}	GPa	5	3
G_{23}	GPa	4.2	3
ν_{12}	-	0.3	0.05
ν_{13}	-	0.3	0.05
ν_{23}	-	0.4	0.05

Table 4-1: Stiffness properties attributed to orthotropic material models

Cooling analyses have been performed by using the Abaqus/Standard code. The centre of gravity of the specimen has been constrained and a temperature variation of 160°C (from an initial condition of 180°C to a final temperature of 20° C) has been imposed. A sensitivity analysis to the coefficient of thermal expansion of the composite material has been performed, whereas the CTE of the titanium alloy has been kept to $9 \cdot 10^{-6}$ C^{-1}, as used in preliminary analyses. The numerical evolution of strain vs. temperature is uniform in large part of the specimen and, in particular, at all the locations corresponding to the position of the FBG sensors in the physical laminate. The results reported in Fig. 4-2-A compare the numerical and the experimental strain vs. temperature curves for the co-bonded type A hybrid laminate. Results indicate that the simplified numerical model of the cooling phase overestimates the contraction of such specimen, even if CTE in fibre direction is set to negative values lower than those indicated by the producer. It should be observed that the

sensors are embedded in the composite, whereas the overall contraction predicted in the model is influenced by the CTE of titanium alloy, which is assumed to be perfectly bonded to the composite UD sub-laminate. Indeed, the presence of adhesive at all interface locations, which could be characterized by a non-negligible viscous response at high temperature, could have allowed a relative motion between metallic and composite layer, so that the contraction of the composite resulted lower than the one referred to a perfect adhesion condition in the hybrid element. Such hypothesis is consistent with the non-linearity of experimental strain vs. temperature curves. The hypothesis is also confirmed by the numerical-experimental correlation obtained in the co-cured specimens type B, with fabric sub-laminates and no adhesive, reported in Fig. 4-2-B, where a good numerical-experimental correlation has been obtained by adopting the CTE values indicated in material datasheet.

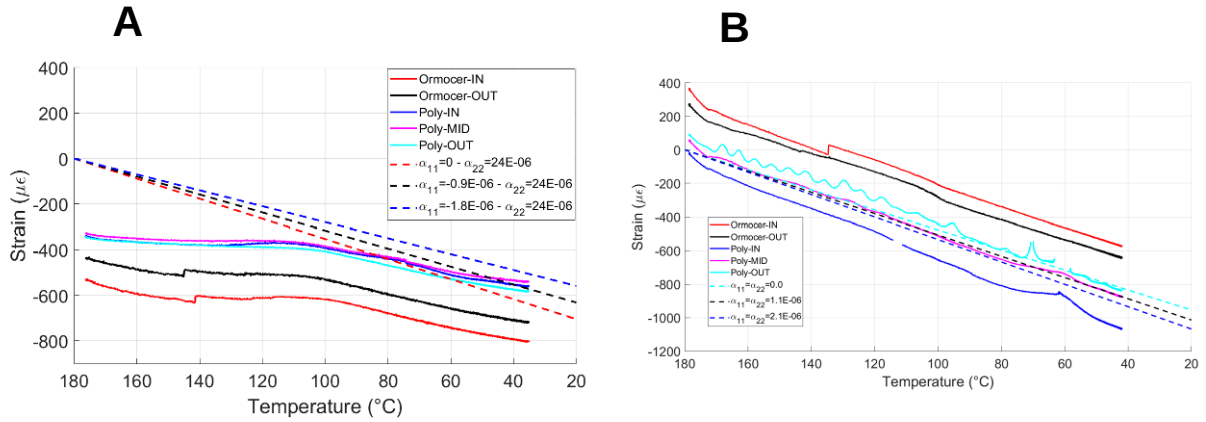

Figure 4-2: Numerical-experimental correlation of strain evolution in the cooling phase for Ti-UD co-bonded specimens (A) and Ti-FB co-cured specimens (B)

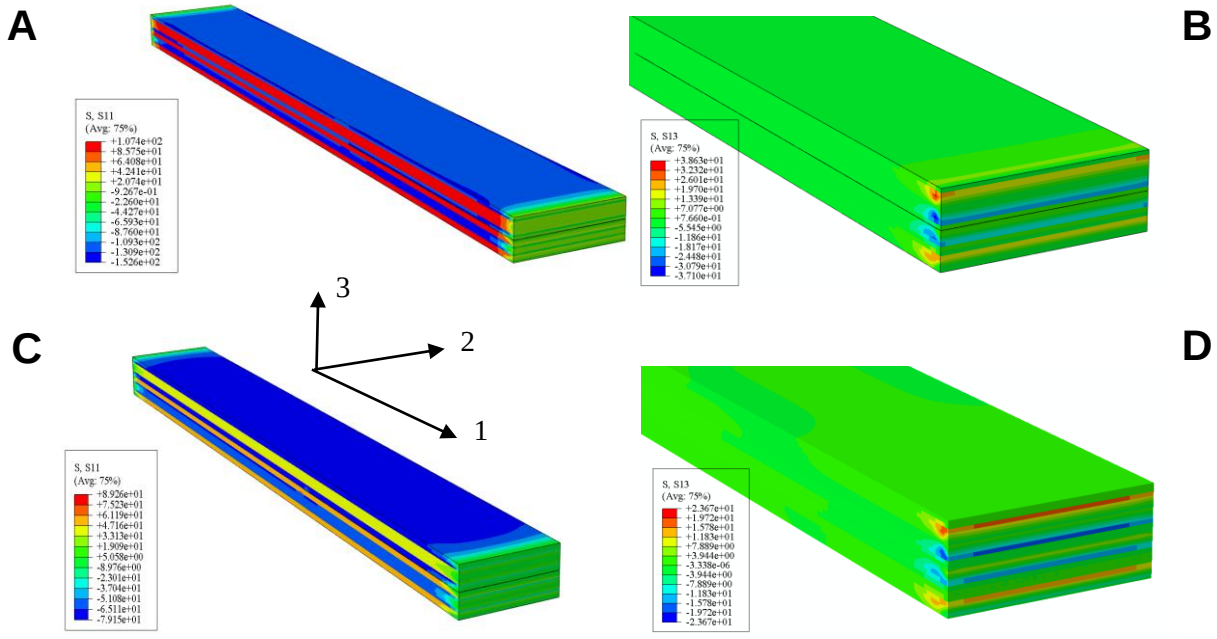

Figure 4-3: Numerical normal stress σ_{11} (A) and τ_{13} (B) for the analysis of co-bonded Ti-UD specimen and of normal stress σ_{11} (C) and τ_{13} (D) for the analysis of co-cured TI-FB specimens

Further results of thermal analyses are reported in Fig. 4-3, which is referred to the contour of longitudinal normal stress and transverse shear stress for the specimens with co-bonded unidirectional sub-laminates and

co-cured fabric sub-laminates. The values reported in Fig. 4-3-A indicate that compressive stress between 110 MPa and 130 MPa are obtained in the composite layers, whereas the tensile stress in titanium alloy are about 100 MPa. Such stress states are transmitted at the end of the specimen by interface shear stress, which are shown in Fig. 4-3-B and can reach levels up to 38 MPa. Following the previous considerations derived from numerical-experimental correlation of strain, such stress state is probably overestimated. However, both the experimental and the numerical analyses confirm that no shape distortion are induced during the cooling phase, thanks to the specimen design. For the hybrid specimen with co-cured fabric sub-laminates, results reported in Fig. 4-3-C and Fig. 4-3-D indicate that compressive normal longitudinal stress between 65 MPa and 80 MPa are reached in the titanium layers, whereas the stress in fabric sub-laminates are tensile, with values in the range 30 MPa ÷ 60 MPa. The maximum transverse shear stress at the end of the specimens are about 24 MPa and are lower than the ones achieved in the numerical analysis referred to unidirectional sub-laminates, but it has to be remarked that the very poor toughness properties of co-cured interface suggest a very low strength levels, so that the predicted stress could lead to the development of damage at the interface during the cooling phase of the process.

4.2 Modelling of global response and local strain evolution in DCB tests

The same models used for the thermal analyses can be adopted in the simulation of the DCB tests. The extremely low toughness properties and the interface stress levels predicted for the specimens with fabric sub-laminates suggested that further studies were required before undertaking the simulation of DCB fracture process. Accordingly, finite element analyses have been conducted considering the DCB tests performed on the UD specimens, with the aim of validating the numerical model of the specimens in terms of overall force vs. displacement response and of local strain fields in the points monitored by the FBG sensors.

Therefore, the model presented in Fig. 4-1 has been adopted for a separate DCB analysis referred to type A specimen, which has been carried out by using Simulia/Abaqus Explicit code. Two set of nodes have created on the top and lower surface of the upper and lower arm, respectively, in correspondence of the parts bonded to the hinges shown in Fig. 4-4-A, which have been used to apply the loads in the DCB experiment. In the FE models, the two surface node sets have been assigned to two rigid bodies having reference nodes positioned at the centres of the physical hinge. A quasi-static explicit analysis has been performed, by smoothly increasing the vertical velocity that has been assigned in the upward and downward direction to the reference node, so to simulate the opening of the specimen, as shown in Fig. 4-4-B, which reports the contour of longitudinal stress in the specimen. The damage propagation at the co-bonded interface has been represented by properly characterized cohesive elements, set between the solids elements that model the titanium layer and the unidirectional sub-laminate at the mid-plane. Cohesive elements are 8-noded elements with zero or very small thickness that can be used to join solid elements and model both the strength and the toughness of an interface by means of a traction-separation law, which evaluate the stress transmitted through the interface as a function of the discontinuity between the displacements $\boldsymbol{u}^+$ and $\boldsymbol{u}^-$ shown in Fig. 4-5-A. The typically used traction-separation law, shown in Fig. 4-5-B, is bi-linear, though more complex responses are required to model R-curve effects, when toughness is a function of crack length (see, for instance, [23]). In the bi-linear law, maximum stress level determines the point of damage onset and model the strength, whereas the area below the traction-separation response define the critical energy release rate required to completely open a new unit surface at the interface. Separate laws are introduced for mode I, mode II and mode III opening, which interact by means of stress and toughness criteria for generic mixed mode phenomena [27]. Since the DCB test is a pure mode I test, mode II and mode III properties do not have influence on the results and have been set equal to the those of mode I, indicated in Table 4-2. The penalty stiffness K is a fundamental parameter for cohesive elements and should be calibrated on the basis of numerical considerations. The values adopted in this work have been obtained by applying the formulation propose in [28].

Property	Units	Numerical value	Notes
σ_{I0}	GPa	70	Strength from producer data sheet
G_I	kJ/m^2	3.2	From MBT/MCC data reduction
K	GPa/mm	124740	From method reported in [28]

Table 4-2: Parameter of Cohesive zone model

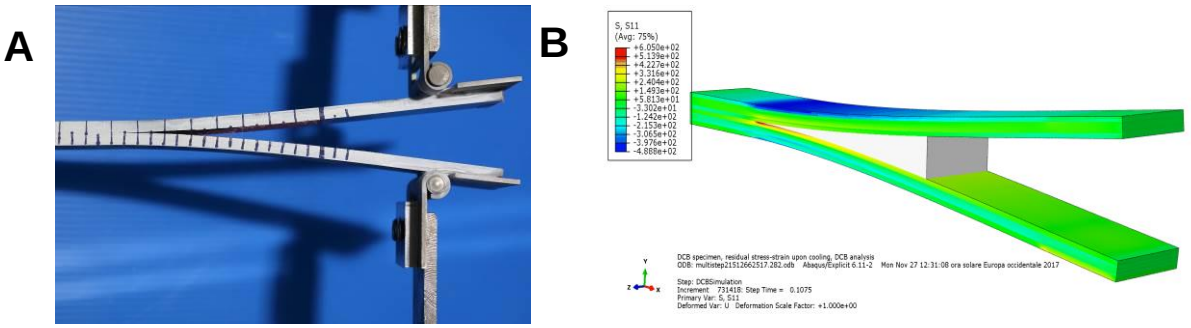

Figure 4-4: Correlation between the experimental deformed shape (A) and the numerical one (B) in the DCB test for the co-bonded hybrid specimens with unidirectional sub-laminates

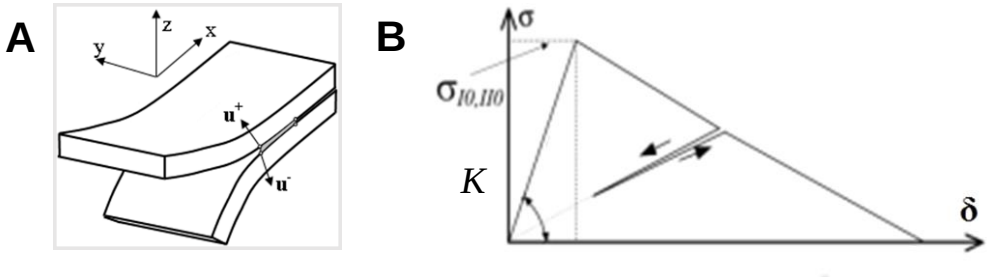

Figure 4-5: Modelling technique for interface damage with cohesive elements (A) and bi-linear traction-separation cohesive zone model (B)

The numerical-experimental correlation of force vs. opening response reported in Fig. 4-6 indicates that the stiffness in the elastic range and the peak of force are predicted with appreciable accuracy. In the softening phase, corresponding at the crack propagation, numerical curve is initially in very good agreement with experiments, but tend to be underestimate as the opening and the crack length increase. Indeed, such aspect is a consequence of the increment of energy release rate, pointed out in Fig. 3-6, since a bilinear cohesive traction-displacement law typically models a constant energy release rate during crack opening. The visual identification of the crack advancement in the test provides an experimental curve a-δ that can be correlated with its numerical counterpart, evaluated considering the longitudinal length of the surface modelled by cohesive elements where damage has reached the unit value. It can be observed, in Fig. 4-6-A that such correlation provides appreciable results, considering the crack length taken at edge of the specimen. The model is also able to capture the curved shape of the crack front, which is a consequence of the anti-clastic curvature of the specimen arms, as it is shown in Fig. 4-7-B.

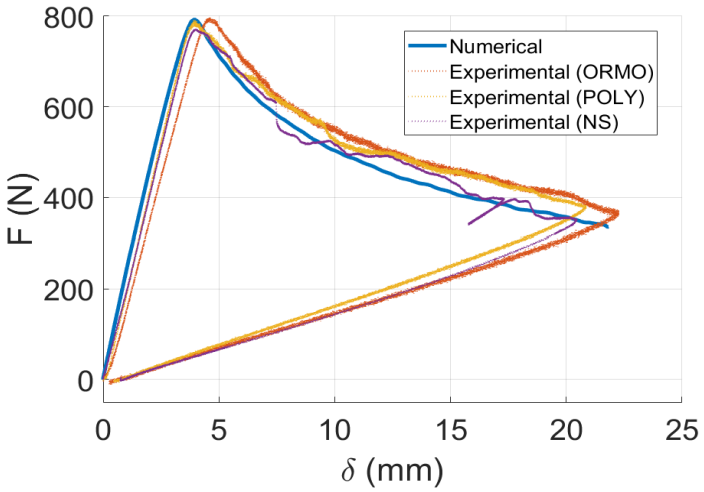

Figure 4-6: Numerical-experimental correlation of force vs. displacement response in DCB test

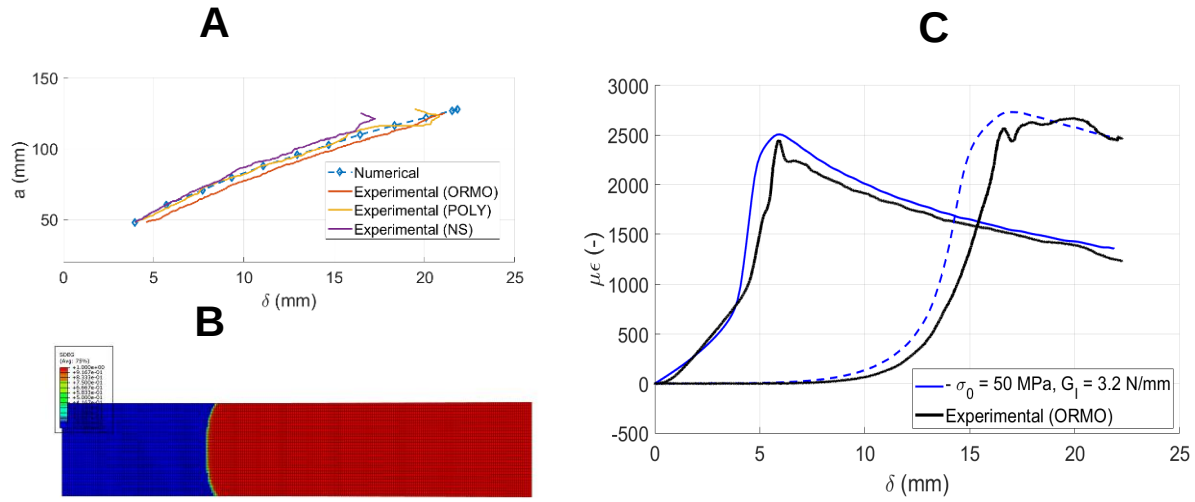

Figure 4-7: Numerical-experimental correlation of crack advancement vs. specimen opening (A), numerical crack front (B) and numerical-experimental correlation of internal strains (C)

Finally, the presence of FBG sensors provides the possibility of a further insight in the deformation process, since the strain signals can be correlated to the numerical strains taken at the same location, averaging the local values at the integration point of all the elements in the length occupied by the FBG's (3 mm). The results provided in Fig. 4-6-C indicate that an acceptable correlation between the evolution of strains at the FBG sensors is achieved. Generally, it can be said that the detail of such local behaviour are influenced by the real distribution of cohesive forces, so that further studies regarding the adoption of different cohesive law shapes are required to improve the correlation.

4.3 Multiple step approach to model thermal stress evolution during cooling and fracture propagation phenomena

The possibility offered by the Simulia/Abaqus code have been exploited to perform a multi-step analyses, so to include the thermal residual stress predicted in the cooling analyses in the initial conditions of the analysis related to fracture testing. The operation is conveniently performed by adopting an explicit time integration

scheme for both the step phases and by varying the boundary conditions through the multiple step analyses as indicated in Fig. 4-8. The model has been characterized by using the same thermo-mechanical properties reported in the previous sub-sections. The main difference in the combined thermo-mechanical and fracture analysis is represented by the presence of the rigid bodies on the external surfaces of the arms, which do not exist during specimen manufacturing and influence the numerical development of thermal stress at the front end of specimen. However, the region interested to such alteration is quite far from the initial crack position, so that the behaviour in the subsequent fracture analysis is not affected. The strain vs. temperature response reported in Fig. 4-9-A has been obtained in the cooling explicit analysis and results are identical to the one of the implicit separate cooling analysis (see Fig. 4-2). Considering the force vs. overall response in the DCB analysis, shown in Fig. 4-9-B, the numerical curve presents the same trend of the implicit results, though a series of low amplitude oscillations can be observed in the crack propagation phase. The correlation of the strains measured by the FBG sensor, provided in Fig. 4-10, indicates that also at the local level the multiple step proposed methodology provide a reliable prediction of the hybrid structure response, which can take into consideration the presence of thermal stress in the structure.

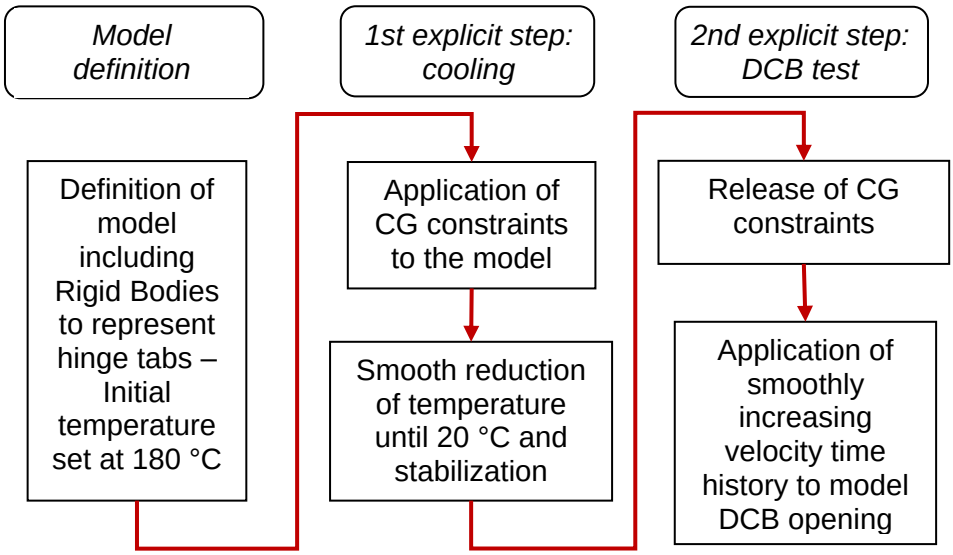

Figure 4-8: Multiple step analysis procedure for cooling and DCB test analyses

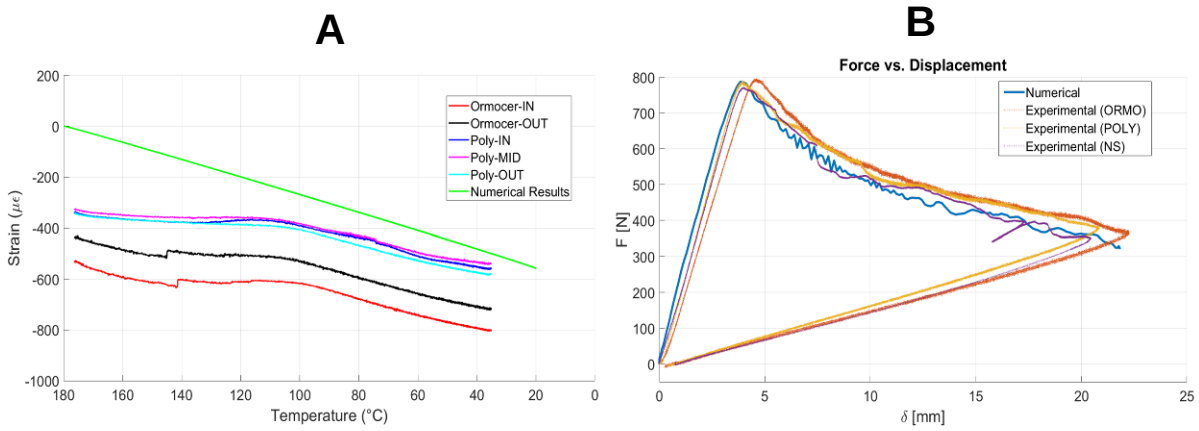

Figure 4-9: Numerical-experimental correlation in the cooling step (A) and in the DCB test step (B) of the

multistep analysis

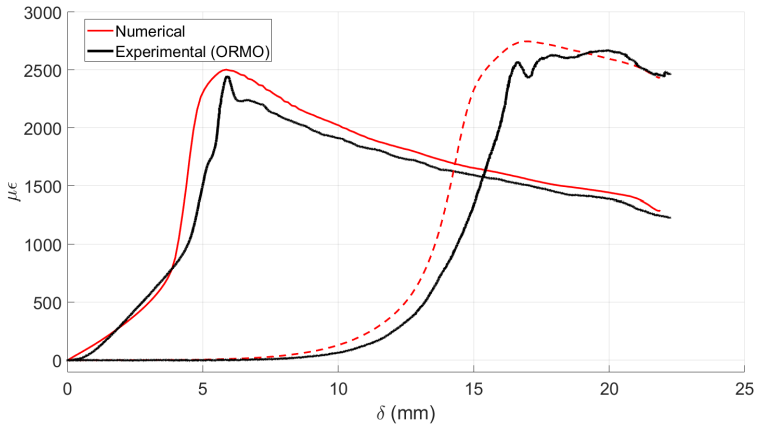

Figure 4-10: Numerical-experimental correlation in the explicit DCB analysis step subsequent to thermal cooling explicit analysis

5.0 CONCLUSIONS

The paper has assessed experimental and numerical approach for the characterization of the fracture toughness of co-cured and co-bonded interfaces in hybrid composite/metallic structures. Such structures can be considered particularly interesting for the application in military fields, since they can combine the superior stiffness to weight ratio of composite materials with the ductility, the toughness and the inherent strength in the presence of 3D stress states that characterize metal parts. The adhesion between the elements of hybrid composite metallic structures is a critical issue and the research performed provides results in several areas.

In particular, the assessment of specimen types to characterize different types of interfaces can be exploited to select the best trade-off between manufacturing complexity and the achievement of the toughness levels that can be required in the severe loading and environmental conditions that characterize military applications. Indeed, the peculiar lay-up devised for the specimens and verified in preliminary analyses proved to be effective in avoiding geometrical distortions due to CTE's mismatch and consequent effects on energy release rate measured in fracture mechanics tests.

The embedment of optical fibres in the composite laminates close to interfaces also provided significant information regarding the manufacturing process. Thanks to the technique based on capillary tubes, it has been possible to easily decouple the temperature and the strain trends from the acquired signals. Interesting results have been given regarding the behaviour of fibres with chemically removed coating and fibres with ceramic coating embedded at interfaces between unidirectional and fabric plies. Indeed. all these sensors experienced initial offsets during the phase of mould closure and initial pressure application, but the behaviour in the subsequent phases of the process was different. In sub-laminates made of unidirectional plies, with optical fibres parallel to fibre reinforcements, all sensors provided the same strain variations after the initial offset. On the contrary, sensors embedded in fabrics exhibited differences during temperature application and splitting of spectra was observed for sensors with coating removed. However, it has to be remarked that the slopes of the strain vs. temperature curves acquired by the different FBG sensors are very similar for all the sensor types, in both type of hybrid specimens considered, thus indicating that fibre optic based monitoring can provide interesting and consistent information about the build-up of thermal stress in the cooling phase of the process.

The system of sensors was also successfully applied to monitor the evolution of internal strains during

fracture process. Such aspect is particularly relevant for application in the hot spots of military vehicles, to easily detect structural damage that can develop during operations under conditions that can difficulty be accurately foreseen in the design phase.

Numerical models have been developed to analyse both the cooling phase of the manufacturing process and the fracture tests. The simplified approach based on linear elastic material and constant CTE parameters proved to be adequate to capture the trend of strains during the cooling part of the process for a co-cured interface, whereas the analysis in the presence of adhesive resulted more critical, and deserve further studies focused on the simulation of adhesive response and of the friction between the specimen and mould. However, multiple step explicit analyses including cohesive zone model proved to be a reliable approach to model both cooling process and subsequent damage evolution, provided that the material and the interfaces are properly characterized. The analyses of fracture mechanics tests obtained acceptable correlations in term of overall force vs. strain response and local strain evolution. It is also significant that the numerical approaches assessed in the paper can potentially model the anomalies in the strain fields originated by interface damage, including the ones due to the release of the thermal stress, so to greatly increase the capability of predicting the actual performances of a strain sensing network embedded in the structure. Such combination between the possibilities offered by optical fibre technology and the numerical prediction of sensing network performances is fundamental to design effective Usage and Health Monitoring System that could represent one of the most important features of future generation military vehicles.

Besides the assessment of experimental and numerical approaches, further results have been obtained. In particular, the largely different toughness of co-cured and co-bonded interfaces has been pointed out by using a reliable experimental technique. Moreover, results indicate the presence of a slight R-curve effect in the toughness properties of co-bonded interfaces, which could be taken into account to improve the correlation of overall force and of strain evolution during a fracture propagation. Finally, the indication regarding the non-linear trend of strain during the cooling process in the presence of the adhesive layer seems involving a mitigation effect of thermal stress build-up, due to possible relaxation viscous effects of the adhesive. Such results confirm the potential of the proposed approach and deserve further investigations regarding the toughness of co-cured interface for different surface preparations, the evaluation of thermal residual strain in co-bonded hybrid elements and the application of the approach to cases where thermal strains are released by crack development, so to make possible a reliable estimation of damage detection probability and the design of strain sensing networks to monitor critical zones at the interfaces of hybrid composite/metallic structures.

ACKNOLEDGEMENTS

The authors thanks Dr. Sara Ghiavsand, sponsored by the EU funded NITROS project, for the contribution provided in the development of numerical models in this work.

REFERENCES

[1] Vlot A., Gunniink J.W., Fibre Metal Laminates: an introduction, 1st ed., Vol 2, *Kluwer Academic Publishers, 2001*.

[2] Cho D.H., Lee D.G., Manufacturing of Co-Cured Composite Aluminum Shafts with Compression during Co-Curing Operation to Reduce Thermal Residual Stress, *Journal of Composite Materials*, Vol. 32, No. 12, 1221-1242.

[3] Lee D.G., Kim H.S., Kim J.W., Kim J.K., Design and manufacture of an automotive hybrid aluminium/composite drive shaft, *Composite Structures*, Vol. 63, 87-99, 2004.

[4] J. Ludick, Raman T., Industrialization of a Carbon Composite Control Rod, *Proceedings of International Conference on Composite Materials, ICCM-12, Paris,* July 1999.

[5] Mara V., Haghani R., Al-Emrani M., Improving the performance of bolted joints in composite structures using metal inserts, *Journal of Composite Materials,* Vol. 50, No. 21, 3001-3018, 2015.

[6] Mazraehshahi H.T., Zakeri A.A., Influence of material and geometrical parameters on stress field of composite plates with inserts, *Proc. IMechE, Vol 226, Part G: Aerospace Engineering,* 1573-1582, 2011.

[7] Camanho P.P., Fink A., Obst A., Pimenta S., Hybrid titanium-CFRP laminates for high-performance bolted joints, *Composite Part A, Applied Science and Manufacturing,* 1826-1837, 2009

[8] Fink A., Camanho P.P., Andrés J.M., Pfeiffer E., obst A., Hybrid CFRP/titanium bolted joints: Performance assessment and application to a spacecraft payload adaptor, *Composite Science and Technology,* Vol. 70(2), 305-317, 2010.

[9] Molnar P., Mitschang P., Felhos D., Improvement in bonding of functional elements with the fiber reinforcement polymer structure by means of tailoring technology, *Journal of Composite Materials,* Vol. 41, No, 21, 2007.

[10] Wisnom M.R., Gigliotti M., Ersoy N., Campbell M., Potter K.D., Mechanisms generating residual stress and distortion during manufacturing of polymer matrix composite structures, *Composites Part A: Applied Science and Manufacturing,* Vol. 37(4), 522-529, 2006.

[11] Parleviet P.P., Bersee H., Beukers A., Residual stresses in thermoplastic composites – a study of literature – part I: formation of resisual stresses, *Composites Part A: Applied Science and Manufacturing,* 37(11), 1847-1857, 2006.

[12] Zobeiry N., Poursatib A. The origin of residual stress and its evaluation in composite materials, in *Structural Integrity and Durability of Advanced Composites,* Beaumont P., Soutis C., Hodzic A. Editors, 1st Edition, Woodhead Publishing 2015.

[13] Kim H.S., Park S.W., Lee D.G., Smart cure cycle with cooling and rehating for co-cure bonded steel/carbon expoxy composites hybrid structures for reducing thermal residual stress, *Composites Part A: Applied Science and Manufacturing,* Vol. 37, 1708-1721, 2006.

[14] Kim H.S., Lee D.G., Reduction of fabricational thermal residual stress of the hybrid co-cured structure using a dielectometry, *Composites Science and Technology,* Vol. 67, 29-44, 2007.

[15] Park S.W., Kim H.S., Lee D.G., Optimum design of the co-cured double lap joint composed of aluminum and carbon epoxy composite, *Composite Structures,* Vol 75, 289-297, 2006.

[16] Lin C.T., Kao P.W., Jen M.-H. R, Thermal residual strains in carbon fibre-reinforced aluminum laminates, *Composites,* Vol. 25, No. 4, 303-307, 1994.

[17] Hausmann J., Naghipur P., Schulze K., Analytical and numerical residual stress models for fiber metal laminates – comparison and application, *Procedia Materials Science,* Vol 2, 68-73, 2013.

[18] Sorensen L., Gmür T., Botsis J., Residual strain development in lamianted thermoplastic composites measured using fibre Bragg grating sensors, *Proceedings of CompTest 2004 conference, Bristol, UK, September 21-23,* pp- 145-146, 2004.

[19] Parleviet P.P., Bersee H., Beukers A., Residual stresses in thermoplastic composites – a study of literature – part II: experimental techniques, *Composites Part A: Applied Science and Manufacturing*, 38(3), 651-665, 2007.

[20] Sala G., Di Landro L., Airoldi A., Bettini P., Fibre optic health monitoring for aeronauical applications, *Meccanica*, Vol. 50(10), 2547-2567, 2015.

[21] Grattan K., Sun T., Fiber optic sensor technology: an overview. *Sensors and Actuators A: Physical*, Vol. 82(1), 40-61, 2000.

[22] Wisnom M.R., Modelling discrete failures in composites with interface elements, *Composite Part A: Applied Science and Manufacturing, Vol. 41, 795-805, 2010*.

[23] Airoldi A., Baldi A., Bettni P., Sala G., Efficient modelling of forces and local strain evolution during delamination of composite laminates, *Composites: Part B.* Vol. 72, 137-149, 2015.

[24] Montanini R., D'Acquisto L., Simulateneous measurement of temperature and strain in glass fiber/epoxy composites by embedded fiber optic sensors: I. cure monitoring, *Smart Materials and Structures* 16(5): 1718, 2007.

[25] ASTM D5528-01. Standard Test Method for Mode I Interlaminar Fracture Toughness of Unidirectional Fiber-Reinforced Polymer Matrix Composites. Annual Book of ASTM Standards. West Conshohocken (PA, USA): *American Society for Testing and Materials;* 2002.

[26] Dassult Systemes Simulia Corporation, Abaqus, 2012 Analysis User Maual Version 6.12, Providence, RI. USA, 2012.

[27] Camanho P.P., Dávila C.G., de Moura M.F.S.F., Numerical simulation of mixed-mode progressive delamination in composte materials, *Journal of Composite Materials*, Vol. 37(16), 1415-1438, 2003.

[28] Turon A., Dávila C.G., Camanho P.P., Costa J., An engineering solution for mesh size effect in the simulation of delamination using cohesive zone models, *Engineering Fracture Mechanics*, Vol. 74 1665-1682, 2007.